Zinc Complex Based Multifunctional Reactive Lithium Polysulfide Trapper Approaching Its Theoretical Efficiency

Zhong Ma
University of Waterloo
Zhijun Zuo
Taiyuan University of Technology
Yuning Li (yuning.li@uwaterloo.ca)
University of Waterloo https://orcid.org/0000-0003-3679-8133

Research Article

Keywords: Lithium sulfur battery, lithium polysulfide, shuttle effect, polysulfide trapping, cycling stability, catalysis

Posted Date: November 14th, 2020

DOI: https://doi.org/10.21203/rs.3.rs-108229/v1

Version of Record: A version of this preprint was published at ACS Applied Materials & Interfaces on May 13th, 2021. See the published version at https://doi.org/10.1021/acsami.1c04483.

Abstract

The “shuttle effect” of soluble lithium polysulfides (LPS), which causes rapid capacity fading, remains a lingering issue for lithium-sulfur batteries (LSBs). Herein, we report a new type of reactive molecule-based (or molecular) LPS trapper, zinc acetate-diethanolamine ($Zn(OAc)_2$·DEA), which demonstrated a molecular efficiency of 1.8 for LPS trapping, approaching its theoretical limit of 2. This is the highest trapping capability among all reported LPS trappers. During discharge the trapped polysulfides are much more thermodynamically favored for reduction compared to the non-trapped ones, while during charge the complex $Zn(SLi)_2$·DEA formed in the previous discharging process can be more easily oxidized due to its lower energy barrier in comparison to Li_2S, indicating the catalytic effects of Zn^{2+}·DEA on the redox of sulfur species. $Zn(OAc)_2$·DEA is also an excellent binder owing to its multiple intermolecular hydrogen bonds. LSBs using $Zn(OAc)_2$·DEA as a LPS trapper, a binder, and a redox catalyst exhibited excellent long-term cycling stability (with a capacity retention of 85% after 1000 cycles at a rate of 0.5 C) and enhanced rate performance. The work demonstrated the potential of this novel type of multifunctional metal complex-based reactive molecular LPS trappers for high capacity and stable LSBs.

Introduction

The escalating demand for high energy density rechargeable batteries has not only driven the research on the improvement of traditional lithium ion batteries, but also spurred the development of next generation ultra-high energy density battery technologies such as lithium-oxygen and lithium-sulfur batteries (LSBs)[1,2]. In particular, LSBs possessing a high theoretical specific energy of 2600 Wh kg^{-1} together with the very low cost of sulfur have attracted extensive attention for energy storage applications in recent years[1,3-6]. However, there are still numerous issues that impede commercializing LSBs. One of them is the so-called “shuttle effect”[7], whereas soluble long-chain lithium polysulfides (LPS, Li_2S_x, $4 \leq x \leq 8$) intermediates produced during discharge diffuse to and react with the Li anode to form an insoluble and insulating Li_2S layer on the anode surface[8-10]. This causes continuous loss of active sulfur and an increased impedance of the anode surface, leading to fast fading of battery performance. On the other hand, the formation of soluble LPS is also considered necessary for increasing sulfur utilization and thus a higher specific capacity through a promotion of their subsequent reactions to produce shorter lithium sulfides (Li_2S_2 and Li_2S)[11].

To tackle the “shuttle effect”, numerous efforts have been devoted to explore various materials that can keep or trap the soluble LPS within the sulfur cathode. Mesoporous carbon materials were firstly employed to trap LPS through the spatial confinement and the physical adsorption of LPS on the large surface area of these carbon materials; however, due to the weak intermolecular interaction, LPS readily diffuse out of the pores and the battery capacity degrades rapidly within tens of cycles[3]. It was found that incorporation of heteroatoms such as N[12], O[13] and B[14] in carbon materials can significantly enhance their LPS trapping capabilities due to the strong polar-polar interactions between these heteroatoms and

LPS. Organic polymers and frameworks containing heteroatoms have also shown good LPS trapping effects[9,15,16]. Many metal compounds such as metal oxides[17], sulfides[18], nitrides,[19] and carbides[20] exhibit strong polar-polar interactions between the metal cations (or anions) in these compounds and the S_x^{2-} (or Li^+) ions in LPS[21]. Some metal compounds such as metal-organic frameworks (e.g. the Ni-based MOF)[22] and MXenes (e.g. Ti_2C)[23] have even stronger interactions with LPS to form metal-sulfur chemical bonds.

Nonetheless, since the previously reported LPS trappers are solid aggregates the adsorption of LPS occurs on the surface and thus the quantity of immobilized LPS critically relies on the available surface area of the trappers[24]. Although the surface to volume ratio can be increased laboriously by reducing the particle size or making mesoporous structures[25,26], there would be always a large portion of inaccessible materials and a large amount of LPS trappers are required to achieve a satisfactory battery lifetime. Furthermore, most of the LPS trappers are incorporated as additives in the cathode in addition to the required components, i.e., sulfur, conductive carbon and binder. Consequently, the use of these known LPS trappers would inevitably reduce the sulfur content in the cathode and thus the energy density of LSBs[27].

In this study, we report the use of a simple organometallic compound, zinc acetate-diethanolamine complex ($Zn(OAc)_2$·DEA) as a new type of reactive molecular LPS trapper, which showed an ultra-high mass trapping efficiency (η_m) of 1.3 $g_{LPS}\ g_{trapper}^{-1}$ (LPS = Li_2S_6, trapper = $Zn(OAc)_2$·DEA). This value is equivalent to 1.8 LPS molecules being trapped by each $Zn(OAc)_2$·DEA molecule, or a "molecular efficiency (η_n)" of 1.8 $mol_{LPS}\ mol_{trapper}^{-1}$, which approaches the theoretical limit of 2 $mol_{LPS}\ mol_{trapper}^{-1}$ for $Zn(OAc)_2$·DEA, indicating that almost all $Zn(OAc)_2$·DEA molecules can participate in the LPS trapping. Both the mass and molecular trapping efficiencies of $Zn(OAc)_2$·DEA far exceed those of the LPS trappers reported so far. It was found that the S_x^{2-} anions of LPS formed in the cathode during discharge spontaneously replace the acetate anions in $Zn(OAc)_2$·DEA to form $Zn(S_xLi)_2$·DEA, while during charge $Zn(OAc)_2$·DEA is regenerated with the release of sulfides and replenishment of acetate anions. This regenerative process maintains the LPS trapping ability of $Zn(OAc)_2$·DEA and achieves high sulfur utilization during long-term cycling. In addition, $Zn(OAc)_2$·DEA showed notable catalytic effects to promote the reactions of sulfur species in both discharge and charge processes. Furthermore, $Zn(OAc)_2$·DEA has strong multiple intermolecular hydrogen bonds to form a 3-dimensional (3D) network, which eliminates the need of an additional binder material. Therefore, the sulfur cathode composite using $Zn(OAc)_2$·DEA as a LPS trapper, a binder, and redox catalyst showed excellent cycling stability, high rate performance, and low self-discharge.

Results

Synthesis and characterization of $Zn(OAc)_2$·DEA

The $Zn(OAc)_2$·DEA complex was conveniently prepared by mixing zinc acetate and DEA with a molar ratio of 1:1 in ethanol at room temperature without purification. Its ^1H NMR spectrum (Fig. 1A and Fig. S1A) showed three peaks at 1.98, 2.95 and 3.75 ppm with integral ratios of 3:2:2, which are assigned to the H atoms in CH_3, CH_2-N and O-CH_2, respectively[28]. There were no observable starting materials and other impurities, indicating the quantitative formation of $Zn(OAc)_2$·DEA (Fig. S2A-B). Previous single crystal XRD studies revealed that each $Zn(OAc)_2$·DEA molecule forms six hydrogen bonds with two neighboring $Zn(OAc)_2$·DEA molecules, which include 2 ´ O-H···O=C (1.792Å), 2 ´ O-H···O-Zn (1.918 Å), and 2 ´ N-H···O=C (2.294Å) (Fig. S1B-C)[28]. These multiple hydrogen bonds would form a 3D interconnected network in the $Zn(OAc)_2$·DEA solid. The rather flexible DEA ligands and reversible formation and dissociation of hydrogen bonds make $Zn(OAc)_2$·DEA a potential “self-healable” sulfur cathode binder that can cushion the large volume change (up to 80%) of sulfur species between charge and discharge to maintain the structural integrity of the sulfur cathode. It is noticed that there exist large spaces between neighboring $Zn(OAc)_2$·DEA molecules, which would make polysulfide anions accessible to the Zn^{2+} cations for the facile entrapment of LPS.

Electrochemical performance of $Zn(OAc)_2$·DEA based sulfur electrode

To test the ability of $Zn(OAc)_2$·DEA as a binder, it was mixed with Super P with a mass ratio of 1:3.6 in a mixture of ethanol and water (*v:v* =1:1). A very uniform slurry with excellent coating properties was obtained. The XRD pattern of a dried $Zn(OAc)_2$·DEA/Super P sample from the slurry showed no obvious diffraction peaks originated from $Zn(OAc)_2$·DEA, indicating that $Zn(OAc)_2$·DEA was well dispersed in the blend (Fig. S3). Accordingly, we prepared the sulfur cathode slurry using elemental sulfur as active material, Super P as conductor, and $Zn(OAc)_2$·DEA as binder with a mixture solvent of ethanol and water (*v:v* =1:1), which showed a very good film forming property, comparable to that prepared using PVDF as binder in *N*-methyl-2-pyrrolidone (NMP) (Fig. S4). The electrochemical performance of $Zn(OAc)_2$·DEA based electrode was then evaluated in comparison to the PVDF based electrode.

As shown in Fig. 2A, the CV profile of the $Zn(OAc)_2$·DEA based cathode at a scan rate of 0.1 mV s^{-1} showed the typical two pairs of cathodic/anodic peaks, corresponding to the two-step reversible redox reaction between elemental sulfur (S_8) and Li_2S[29,30]. The PVDF based cathode also showed two pairs of redox peaks; however, both reduction and oxidation peaks, particularly the second reduction and oxidation peaks, are much delayed. This indicates that the redox kinetics of sulfur species in the $Zn(OAc)_2$·DEA based electrode is enhanced[31,32]. A cell containing $Zn(OAc)_2$·DEA and Super P (1:1) without sulfur was also cycled under the same conditions, which showed that $Zn(OAc)_2$·DEA is stable in the potential range of 1.7-2.8 V that is the typical charge/discharge potential range for LSBs (Fig. S5A). When the $Zn(OAc)_2$·DEA electrode was cycled on a battery tester at 0.1 C, it exhibited an initial specific discharge capacity of 1170 mAh g^{-1}, which increased by 14% compared to the PVDF based electrode

(1025 mAh g^{-1}) (Fig. 2B). The former also showed a higher capacity in the first discharge plateau (388 mAh g^{-1} vs. 340 mAh g^{-1}) (Fig. S5B), indicating its higher sulfur utilization[33]. Besides, the discharge-charge plateau gap for the $Zn(OAc)_2$·DEA electrode is only 143 mV, much smaller than that (200 mV) for the PVDF based electrode, implying its fast reaction kinetics[18], which agrees with the CV results. Furthermore, no obvious valley between the first and second plateaus was observed in the discharge curve of the $Zn(OAc)_2$·DEA based electrode, while there is a large overpotential of 39 mV for the PVDF based electrode, which suggests that the interfacial energy barriers for the nucleation and deposition of Li_2S were reduced in the $Zn(OAc)_2$·DEA based electrode (Fig. S5B)[34]. At 0.2 C, the $Zn(OAc)_2$·DEA based electrode achieved a capacity retention of 95% after 100th cycles, which is a significant improvement compared to that (57%) for the PVDF based electrode (Fig. 2C). Moreover, a much improved rate performance with capacity ~800 mAh g^{-1} at a rate of 2 C was obtained for the $Zn(OAc)_2$·DEA based electrode due to its enhanced reaction kinetics (Fig. 2D). More importantly, the $Zn(OAc)_2$·DEA based electrode demonstrated an excellent long-term cycling stability with a capacity retention of 85% after 1000 cycles at a rate of 0.5 C, which corresponds to a very low capacity fading rate of 0.015% per cycle (Fig. 2E). Additionally, the open circuit potential (OCP) of the $Zn(OAc)_2$·DEA based battery was also very stable, achieving 99% retention after ten days, while the PVDF based battery only had 82% OCP retention, indicating the much lower self-discharge of the former (Fig. S5C)[35].

Interactions between $Zn(OAc)_2$·DEA and LPS

The greatly enhanced cycling stability of the $Zn(OAc)_2$·DEA based electrode is considered to be mainly contributed by the efficient LPS trapping capability of $Zn(OAc)_2$·DEA. To quantify the LPS trapping capability of $Zn(OAc)_2$·DEA, an ultraviolet-visible (UV-vis) spectrometer was used to measure the supernatant solutions of the $Zn(OAc)_2$·DEA/Super P composite with addition of different amounts of Li_2S_6 in the same solvent used for the battery electrolyte, 1,3-dioxolane/1,2-dimethoxyethane (DOL/DME, *v*:*v* = 1:1) (Fig. S6 and Table S1)[24]. The commonly used parameters to describe the LPS trapping capability, such as $g_{LPS}\ m_{trapper}^{-2}$ and $g_{LPS}\ g_{trapper}^{-1}$, are not very suitable for evaluating the trapping capability of a molecular LPS trapper, like $Zn(OAc)_2$·DEA. Therefore, we defined the "molecular efficiency (η_n)", i. e., the number of molecules (or moles) of LPS trapped by one molecule (or mole) of LPS trapper, as a new parameter for the evaluation of the LPS trapping capability of molecular LPS trappers (see the more detailed definition of η_n in the Supporting Information). The molecular efficiency h_n of $Zn(OAc)_2$·DEA for trapping Li_2S_6 was calculated from the UV-vis absorption data to be 1.8 $mol_{LPS}\ mol_{trapper}^{-1}$, i. e., each $Zn(OAc)_2$·DEA molecule is capable of trapping 1.8 LPS molecules. This corresponds to a high mass efficiency (h_m) for LPS trapping of 1.3 $g_{LPS}\ g_{trapper}^{-1}$. The LPS trapping capability of $Zn(OAc)_2$·DEA far exceeds those of all LPS trappers reported so far (Table S2 and Fig. S7).

The LPS trapping mechanism of $Zn(OAc)_2$·DEA was studied by using ^1H NMR by adding a Li_2S_6 solution in DOL/DME to a $Zn(OAc)_2$·DEA solution in deuterated methanol (CD_3OD). When one molar equivalent (eq.) of Li_2S_6 was added, white precipitates formed immediately (see the movie in S1 and the photo in Fig. S8A). When adding 2 eq. of Li_2S_6, the solution firstly became turbid, which is similar to that with addition of 1 eq. of Li_2S_6, but soon turned into a clear yellow solution (see the movie in S2 and the photo in Fig. S8B). The ^1H NMR spectrum of the obtained solution of $Zn(OAc)_2$·DEA:2 Li_2S_6 (Fig. 1A) showed the complete disappearance of the peaks H_a and H_b, which belong to $Zn(OAc)_2$·DEA, and the appearance of two new peaks $H_{a'}$ and $H_{b'}$, which can be assigned to the DEA ligand. The peak originated from two acetate anions shifted from 1.98 ppm (H_c) for $Zn(OAc)_2$·DEA to 1.90 ppm ($H_{c'}$) for $Zn(OAc)_2$·DEA:2 Li_2S_6, indicating the formation of lithium acetate in the latter (Fig.S2C). Furthermore, the integral ratios of $H_{a'}$: $H_{b'}$:$H_{c'}$ are 2:2:3 indicate that the two acetate anions in each $Zn(OAc)_2$·DEA complex were completed removed by 2 eq. of Li_2S_6. With further increasing the amount of Li_2S_6 (up to 7 molar eq.) no noticeable changes in the ^1H NMR spectrum of the resulting mixture of $Zn(OAc)_2$·DEA and Li_2S_6 were observed (Fig. S9). Based on the above NMR data, it is most likely that a reaction proposed in Fig. 1B occurred, that is, each $Zn(OAc)_2$·DEA reacted with or trapped two Li_2S_6 molecules to form a complex $Zn(S_6Li)_2$·DEA, which agrees well with the result obtained with UV-vis spectroscopy. We also mixed $Zn(OAc)_2$·DEA with 2 eq. Li_2S in CD_3OD and observed the formation of white precipitates immediately (see movie S3 and Fig. S10A), indicating that Li_2S can readily react with $Zn(OAc)_2$·DEA as well. The ^1H NMR spectrum of the reaction mixture (Fig. S10B) also showed the release of two lithium acetate molecules, indicating that $Zn(SLi)_2$·DEA possibly formed (Fig. S10C). When this reaction mixture was further mixed with 2 eq. of Li_2S_6, most of the white precipitates disappeared and a slightly turbid yellow solution resembling that of $Zn(S_6Li)_2$·DEAwas obtained (movie S4 and Fig. S11A). The NMR spectrum of this solution (Fig. S11B) indeed showed the formation of $Zn(S_6Li)_2$·DEA, indicating that Li_2S_6 can readily react with $Zn(SLi)_2$·DEA to form $Zn(S_6Li)_2$·DEA with the release of Li_2S. This indicates that $Zn(SLi)_2$·DEA can also trap soluble LPS.

The interactions between $Zn(OAc)_2$·DEA and LPS during discharge and charge were further examined by X-ray photoelectron spectroscopy (XPS). The high resolution XPS spectra of Zn 2p showed a binding energy of 1022.5 eV for the fresh $Zn(OAc)_2$·DEA based electrode (Fig. 3A), which is similar to that of Zn in zinc acetate (Fig. S12). After discharging to 2.2 V and then 1.7 V, the binding energy decreased to 1021.6 eV and 1021.3 eV, respectively, which is most likely due to the formation of Zn-S_x bonds with longer (x = 4-8) and shorter sulfide chains (x = 1), respectively. When the electrode recharged to 2.8 V, the binding energy returned to 1022.2 eV, which is very close to that of the fresh electrode. This indicates that the sulfide anions in $Zn(SLi)_2$·DEA in the discharged cathode were oxidized to form elemental sulfur, while the $Zn(OAc)_2$·DEA complex was regenerated during charge. There is a possibility that instead of acetate anions TFSI or nitrate anions in the electrolyte combine with Zn^{2+}, but the Zn binding energy in $Zn(TFSI)_2$ or $Zn(NO_3)_2$ would be quite different at 1023.1 eV (Fig. S12) and 1021.3 eV[36], respectively, if these

products were formed. After fully discharging to 1.7 V, the S 2p spectra of the cathode showed the formation of Li_2S (71%) with the rest (29%) being Li_2S_2[31,32] and $Zn(SLi)_2$·DEA. The formation of elemental sulfur and complete disappearance of Li_2S were observed after fully recharging to 2.8 V (Fig. 3B)[32]. Surprisingly, a significant amount of Li_2S (13%) was detected in the cathode when the battery was partially discharged to 2.2 V in the first discharge plateau, at which Li_2S should be absent[31,37]. This strongly indicates that formation of Li_2S was promoted in the presence of $Zn(OAc)_2$·DEA.

Based on the above results, we proposed a reaction cycle involving $Zn(OAc)_2$·DEA during the redox (discharge/charge) in the sulfur cathode as shown in Fig. 4. Specifically, when the battery is discharged, the formed LPS (Li_2S_x, $4 \leq x \leq 8$) readily replace the acetate anions in $Zn(OAc)_2$·DEA, forming a new complex $Zn(S_xLi)_2$·DEA (I). As the discharging process continues, (I) converts to the final complex $Zn(SLi)_2$·DEA (II) along with the formation of Li_2S and Li_2S_2. When the battery is (re)charged, the sulfide (S^{2-}) anions in (II) are oxidized to form elemental sulfur (S_8), while acetate anions come back to Zn^{2+} to regenerate the $Zn(OAc)_2$·DEA complex. The very high η_n of 1.8 mol_{LPS} mol_{trap}^{-1} obtained by the UV-vis measurement, which approaches the theoretical limit of 2 mol_{LPS} mol_{trap}^{-1} for $Zn(OAc)_2$·DEA, indicates that almost all $Zn(OAc)_2$·DEA molecules in the cathode would participate in the LPS trapping. In addition, as revealed by the NMR analysis, (II) may further trap long chain LPS to reproduce (I). The strong and repetitive LPS trapping capability of $Zn(OAc)_2$·DEA largely accounts for the outstanding long-term cycling of the $Zn(OAc)_2$·DEA based LSBs. Additionally, $Zn(OAc)_2$·DEA has the rather flexible DEA ligand and reversible formation and dissociation of intermolecular hydrogen bonds or “a self-healing effect”, which may render it an excellent binder that can cushion the large volume oscillation of sulfur species during cycling, which makes a further contribution to the remarkable battery lifetime.

The influences of $Zn(OAc)_2$·DEA on the redox of sulfur species

The electronic states of the sulfur species in complexes (I) and (II) shown in Fig. 4 may be altered by Zn^{2+} and thus both reduction of LPS to form Li_2S and oxidation of Li_2S to form S_8 are possibly promoted as shown in the CV and galvanostatical test results. To gain an insight into catalytic effects of $Zn(OAc)_2$·DEA on the charge/discharge processes of the sulfur cathode, first-principles density functional theory (DFT) calculations were performed using the Cambridge serial total energy package (CASTEP) code[38].

The discharge process from S_8 and Li to Li_2S involves the formation of different intermediates, namely, Li_2S_8, Li_2S_6, Li_2S_4, and Li_2S_2[30,39]. We propose that corresponding sulfides, $Zn(S_8Li)_2$·DEA, $Zn(S_6Li)_2$·DEA, $Zn(S_4Li)_2$·DEA, and $Zn(S_2Li)_2$·DEA may form during discharge. The geometries of these zinc complexes

and (II) were optimized as shown in Fig. 5A, while the geometries of S_8 and corresponding Li_2S_x are shown in Fig. S13 for comparison. The adsorption conformations of these compounds on the graphene substrate[30], which represents the surface of the conductive carbon, Super P, were also optimized (Fig. S14 and S15). The Gibbs free energy changes (ΔG) for the reduction reactions of sulfur species are denoted as ΔG_1 (S_8 ® S_8^{2-}), ΔG_2 (S_8^{2-} ® S_6^{2-}), ΔG_3 (S_6^{2-} ® S_4^{2-}), ΔG_4 (S_4^{2-} ® S_2^{2-}), and ΔG_5 (S_2^{2-} ® S^{2-}), respectively (see the detailed reactions in Supplementary Information). Fig. 5B shows the Gibbs free energy changes for the reduction reactions of sulfur species with or without Zn^{2+}·DEA. It can be clearly seen that the reactions of sulfur species with Zn^{2+}·DEA have markedly more negative Gibbs free energy changes compared with all the sulfur species without Zn^{2+}·DEA, revealing that the former reactions are thermodynamically much more favored[31]. It should be mentioned that the magnitude of ΔG_1 for the reduction between S_8 and $Zn(OAc)_2$·DEA to form $Zn(S_8Li)_2$·DEA is larger than that for the reduction of S_8 to form Li_2S_8, indicating that the former may occur in the beginning of discharge (as shown in Fig. 4 and Supplementary Information). Furthermore, while the magnitude of ΔG for the reactions without Zn^{2+}·DEA decreases with decreasing the sulfide chain length, that for the ones with Zn^{2+}·DEA remains large. These results indicate that once (I) with long chain sulfides formed, it would be more readily reduced to form a complex with shorter sulfides in comparison to the free sulfides. For the last step reduction from S_2^{2-} to S^{2-}, in particular, the absolute value of ΔG_5 for the formation of $Zn(SLi)_2$·DEA (II) is more than two-fold that of the reduction from Li_2S_2 to Li_2S. This suggests that (II) may form during the first discharge plateau. As shown in the NMR data, (II) may further react with (or trap) LPS to reproduce (I). Li_2S is released in this step, which was observed at a discharge potential of 2.2 V by the XPS measurement, while the newly formed (I) starts a new journey towards (II). Therefore, one $Zn(OAc)_2$·DEA may trap numerous LPS during one discharge.

In the charge process, the regeneration of S_8 may start from the dissociation of Li_2S to yield LiS and Li^+[18,30] (Fig. S16) or the dissociation of (II) to yield $Zn(S_2Li)$·DEA and Li^+ (Fig. 5C). The energy profiles of the dissociation of Li_2S and (II) are shown in Fig. 5D. The dissociation energies of Li_2S and (II) on graphene are 1.77 and 1.81 eV, respectively, indicating that the latter requires a slightly larger net energy to dissociate. However, the energy barrier for the dissociation of (II) is 2.14 eV, which is much lower than that (2.47 eV) for the dissociation of Li_2S, indicating that (II) can be oxidized (or charged) more easily than Li_2S[18]. Once $Zn(OAc)_2$·DEA is recovered, it may react with Li_2S to form (II) again, which can start a new dissociation cycle, or trap longer sulfides during charge. This may interpret the promoted charging process (lower charging potentials) as shown in Fig. 2B. The above DFT calculation results support the enhanced reduction and oxidation kinetics manifested in the longer first discharge plateau, smaller charge/discharge polarization, and excellent high rate performance.

Discussions

$Zn(OAc)_2$·DEA was investigated as a novel type of reactive molecular LPS trapper for LSBs. The UV-vis spectroscopy measurement showed that each $Zn(OAc)_2$·DEA molecule traps 1.8 LPS molecules in average. NMR results indicate that each $Zn(OAc)_2$·DEA molecule can react with two LPS molecules, which suggest that the observed molecular trapping efficiency approaches its theoretical limit of 2 mol_{LPS} $mol_{trapper}^{-1}$. This is the most efficient LPS trapper reported thus far. Furthermore, DFT calculations show that all LPS trapped by $Zn(OAc)_2$·DEA have a much stronger tendency to be reduced to form shorter sulfides, indicating that Zn^{2+}·DEA can catalyze the reduction (or discharge) of sulfur species in the sulfur cathode. On the other hand, NMR analysis proves that the final $Zn(SLi)_2$·DEA can also trap LPS to resume a new reduction cycle. Therefore, one $Zn(OAc)_2$·DEA molecule is capable of trapping and promoting the reduction of multiple LPS molecules during one discharge process. In the charging process, $Zn(OAc)_2$·DEA can be regenerated from $Zn(SLi)_2$·DEA produced in the previous discharge process, which maintains the LPS trapping ability of $Zn(OAc)_2$·DEA and high sulfur utilization during long-term cycling. In addition, $Zn(SLi)_2$·DEA was found to have significantly lower energy barrier for oxidation of S^{2-} than the corresponding Li_2S, suggesting that the charging kinetics is also significantly promoted. Due to the presence of multiple intermolecular hydrogen bonds and the flexibility of DEA ligands, $Zn(OAc)_2$·DEA also functions as a self-healable binder for the sulfur cathode composite to cushion the drastic volume change of the sulfur species during cycling. LSBs using $Zn(OAc)_2$·DEA as a LPS trapper, a binder, and a redox catalyst demonstrated excellent cycling stability, high rate performance, and low self-discharge. This work presented a novel type of metal complex-based multifunctional LPS trapping binders that may open a new venue toward high performance LSBs and possibly other types of batteries with enhanced performance.

$Zn(OAc)_2$·DEA is the first example of this type of LPS trappers. Among the vast number of transition metal-organic ligand complexes that are similar to $Zn(OAc)_2$·DEA, many are potential high efficiency reactive molecular LPS trappers. The molecular efficiency of this type metal complex trappers may be further improved by using transition metals with higher valences, while the use of lighter metals and smaller ligands and anions would further increase the mass trapping efficiency.

Methods

Synthesis of zinc acetate-diethanolamine complex ($Zn(OAc)_2$·DEA). Zinc acetate dihydrate ($Zn(OAc)_2{\cdot}2H_2O$, 5 mmol, 1.097 g) and diethanolamine ($HN(CH_2CH_2OH)_2$, DEA, 5 mmol, 0.526 g) were dissolved in absolute ethanol (10 mL) and the mixture was stirred for 2 h. A transparent $Zn(OAc)_2$·DEA complex solution was obtained, which was used without further purification.

Synthesis of Li_2S_6. Li_2S_6 solution was obtained by heating a mixture of Li_2S and elemental sulfur (S) with a molar ratio of 1:5 in a mixture solvent of 1,2-dimethoxyethane (DME) and 1,3-dioxolane (DOL) (*v*:*v*=1:1) at 80 °C for 12 h under stirring. The Li_2S_6 solution was diluted to 0.5 M for further use.

Fabrication of sulfur electrodes. Sulfur and Super P with a mass ratio of 6:4 were ground together and the mixture was heated at 155 ºC for 12 h to obtain a sulfur/carbon composite. The $Zn(OAc)_2$·DEA binder based electrodes were prepared by coating a slurry containing sulfur/carbon composite and $Zn(OAc)_2$·DEA with a mass ratio of 9:1 in ethanol and deionized water (*v*:*v*=1:1) on a carbon coated aluminum current collector. As comparison, the polyvinylidene difluoride (PVDF) binder based electrodes were prepared in a similar manner except of using PVDF as binder and *N*-methyl-2-pyrrolidone (NMP) as solvent. The coated electrodes were dried in ambient air overnight and then further dried at 50 ºC in an oven overnight. The electrodes were cut into discs with a diameter of 12 mm and dried again at 50 ºC in a vacuum oven for 12 h before being transferred into an argon-filled glovebox. The average sulfur loading on electrodes is 1.5 mg cm^{-2}.

Electrochemical measurements. Electrochemical studies were carried out on 2035 coin cells with lithium foil as anode, Celgard 2400 as separator and 1 M lithium bis(trifluoromethanesulfonyl)imide (LiTFSI) with 2 wt% $LiNO_3$ in a mixture of DME and DOL (*v*:*v*=1:1) as electrolyte. The coin cells were assembled in an argon-filled glove box with both O_2 and H_2O concentrations below 0.5 ppm. The cyclic voltammetry (CV) measurements were conducted in a potential range of 1.7-2.8 V at a scan rate of 0.1 mV s^{-1}. The electrochemical performance of cells was measured galvanostatically in a voltage window of 1.7-2.8 V on a Land 2001A battery test system at different current densities. Electrochemical impedance spectra (EIS) were recorded at the open circuit potential (OCP) using a Bio-logic electrochemical potentiostat/galvanostat (VSP) in a frequency range from 1000 kHz to 0.1 Hz with an AC amplitude of 10 mV. Electrodes under different states for XPS analysis were prepared by discharging/charging the coin cells at the rate of 0.1 C.

Characterization. XRD measurements were carried out on a Bruker D8 Discover X-Ray Diffractometer using Cu Kα radiation (λ = 1.5418 Å). FT-IR analysis was performed on a Bruker Tensor 27 spectrometer. For XPS measurements, the samples were sealed in vials in the glovebox before being quickly transferred to an ultra-high vacuum chamber and measured with Thermo VG Scientific ESCALab 250 using a monochromated Al K-alpha X-ray source. UV-vis absorption spectra were measured on a Cary 7000 Universal Measurement Spectrophotometer (UMS). ^{1}H NMR spectra were collected on a Bruker DPX 300MHz spectrometer.

Theoretical Calculation. The first-principles density functional calculations (DFT) used PW91 functional within the gradient-corrected (GGA) approximation[40] as implemented in the Cambridge serial total energy package (CASTEP) code[38]. The Vanderbilt ultrasoft pseudopotential was used with a cutoff energy of 350.0 eV[41]. Geometric convergence tolerances were set at a maximum force of 0.05 eV/Å, maximum energy change of 2×10^{-5} eV/atom, maximum displacement of 0.002 Å and maximum stress of 0.1 GPa. Density mixing electronic minimizer was implemented and the self-consistent field (SCF) tolerance was set to accuracy of 2×10^{-6} eV/atom for energy convergence. The Gibbs free energy change of each reaction is obtained by subtracting the Gibbs free energy of the reactants from the Gibbs free energy of the products.

Data availability

The data supporting the results of this work are available from the corresponding authors upon reasonable request.

References

1. Bruce, P. G., Freunberger, S. A., Hardwick, L. J. & Tarascon, J.-M. Li-O_2 and Li-S batteries with high energy storage. *Nat. Mater.* **11**, 19-29, (2012).
2. Ma, Z. *et al.* A review of cathode materials and structures for rechargeable lithium-air batteries. *Energy Environ. Sci.* **8**, 2144-2198, (2015).
3. Ji, X., Lee, K. T. & Nazar, L. F. A highly ordered nanostructured carbon-sulphur cathode for lithium-sulphur batteries. *Nat. Mater.* **8**, 500-506, (2009).
4. Manthiram, A., Fu, Y., Chung, S.-H., Zu, C. & Su, Y.-S. Rechargeable lithium-sulfur batteries. *Chem. Rev.* **114**, 11751-11787, (2014).
5. Chen, X., Hou, T., Persson, K. A. & Zhang, Q. Combining theory and experiment in lithium–sulfur batteries: Current progress and future perspectives. *Materials Today* **22**, 142-158, (2019).
6. Liu, F. *et al.* Dual redox mediators accelerate the electrochemical kinetics of lithium-sulfur batteries. *Nat. Commun.* **11**, 5215, (2020).
7. Mikhaylik, Y. V. & Akridge, J. R. Polysulfide shuttle study in the Li/S battery system. *J. Electrochem. Soc.* **151**, A1969, (2004).
8. He, Y. *et al.* Developing a “polysulfide-phobic” strategy to restrain shuttle effect in lithium-sulfur batteries. *Angew. Chem. Int. Edit.* **58**, 11774-11778, (2019).
9. Yan, L. *et al.* Ionically cross-linked PEDOT:PSS as a multi-functional conductive binder for high-performance lithium-sulfur batteries. *Sustain. Energy Fuels* **2**, 1574-1581, (2018).
10. Li, H. *et al.* Suppressed shuttle via inhibiting the formation of long-chain lithium polysulfides and functional separator for greatly Improved lithium-organosulfur batteries performance. *Adv. Energy Mater.* **10**, 1902695, (2020).
11. Mistry, A. N. & Mukherjee, P. P. “Shuttle” in polysulfide shuttle: friend or foe? *J. Phys. Chem. C* **122**, 23845-23851, (2018).
12. Sun, X.-G., Wang, X., Mayes, R. T. & Dai, S. Lithium-sulfur batteries based on nitrogen-doped carbon and an ionic-liquid electrolyte. *ChemSusChem* **5**, 2079-2085, (2012).
13. Ji, L. *et al.* Graphene oxide as a sulfur immobilizer in high performance lithium/sulfur cells. *J. Am. Chem. Soc.* **133**, 18522-18525, (2011).
14. Yang, C.-P. *et al.* Insight into the effect of boron doping on sulfur/carbon cathode in lithium-sulfur batteries. *ACS Appl. Mater. Inter.* **6**, 8789-8795, (2014).

15. Cheng, Z. *et al.* Porous organic polymers for polysulfide trapping in lithium-sulfur batteries. *Adv. Funct. Mater.* **28**, 1707597, (2018).
16. Yan, L. *et al.* A novel epoxy resin-based cathode binder for low cost, long cycling life, and high-energy lithium-sulfur batteries. *J. Mater. Chem. A* **6**, 14315-14323, (2018).
17. Tao, X. *et al.* Balancing surface adsorption and diffusion of lithium-polysulfides on nonconductive oxides for lithium-sulfur battery design. *Nat. Commun.* **7**, 11203, (2016).
18. Zhou, G. *et al.* Catalytic oxidation of Li_2S on the surface of metal sulfides for Li-S batteries. *Proc. Natl. Acad. Sci. USA* **114**, 840-845, (2017).
19. Cui, Z., Zu, C., Zhou, W., Manthiram, A. & Goodenough, J. B. Mesoporous titanium nitride-enabled highly stable lithium-sulfur batteries. *Adv. Mater.* **28**, 6926-6931, (2016).
20. Bao, W., Su, D., Zhang, W., Guo, X. & Wang, G. 3D metal carbide@mesoporous carbon hybrid architecture as a new polysulfide reservoir for lithium-sulfur batteries. *Adv. Funct. Mater.* **26**, 8746-8756, (2016).
21. Balach, J., Linnemann, J., Jaumann, T. & Giebeler, L. Metal-based nanostructured materials for advanced lithium-sulfur batteries. *J. Mater. Chem. A* **6**, 23127-23168, (2018).
22. Zheng, J. *et al.* Lewis acid-base interactions between polysulfides and metal organic framework in lithium sulfur batteries. *Nano Lett.* **14**, 2345-2352, (2014).
23. Liang, X., Garsuch, A. & Nazar, L. F. Sulfur cathodes based on conductive MXene nanosheets for high-performance lithium-sulfur batteries. *Angew. Chem. Int. Edit.* **54**, 3907-3911, (2015).
24. Wu, D. S. *et al.* Quantitative investigation of polysulfide adsorption capability of candidate materials for Li-S batteries. *Energy Stor. Mater.* **13**, 241-246, (2018).
25. Zhou, G. *et al.* Theoretical calculation guided design of single-atom catalysts toward fast kinetic and long-life Li-S batteries. *Nano Lett.* **20**, 1252-1261, (2020).
26. Ma, Z. *et al.* Enhancing oxygen reduction activity of Pt-based electrocatalysts: from theoretical mechanisms to practical methods. *Angew. Chem. Int. Edit.* **59**, 18334-18348, (2020).
27. Xie, Y. *et al.* Semi-flooded sulfur cathode with ultralean absorbed electrolyte in Li-S battery. *Adv. Sci.* **7**, 1903168, (2020).
28. Hayami, R. *et al.* Zinc-diethanolamine complex: synthesis, characterization, and formation mechanism of zinc oxide via thermal decomposition. *J. Sol-gel. Sci. Techn.* **87**, 743-748, (2018).
29. Xu, Z.-L. *et al.* Visualization of regulated nucleation and growth of lithium sulfides for high energy lithium sulfur batteries. *Energy Environ. Sci.* **12**, 3144-3155, (2019).
30. Du, Z. *et al.* Cobalt in Nitrogen-Doped Graphene as Single-Atom Catalyst for High-Sulfur Content Lithium–Sulfur Batteries. *J. Am. Chem. Soc.* **141**, 3977-3985, (2019).
31. Yang, X. *et al.* Promoting the transformation of Li_2S_2 to Li_2S: significantly increasing utilization of active materials for high-sulfur-loading Li-S batteries. *Adv. Mater.* **31**, 1901220, (2019).
32. Liang, X. *et al.* A highly efficient polysulfide mediator for lithium-sulfur batteries. *Nat. Commun.* **6**, 5682, (2015).

33. Kang, N. *et al.* Cathode porosity is a missing key parameter to optimize lithium-sulfur battery energy density. *Nat. Commun.* **10**, 4597, (2019).
34. Park, J. *et al.* The importance of confined sulfur nanodomains and adjoining electron conductive pathways in subreaction regimes of Li-S batteries. *Adv. Energy Mater.* **7**, 1700074, (2017).
35. Wang, L., Liu, J., Yuan, S., Wang, Y. & Xia, Y. To mitigate self-discharge of lithium-sulfur batteries by optimizing ionic liquid electrolytes. *Energy Environ. Sci.* **9**, 224-231, (2016).
36. Rokosz, K. *et al.* SEM, EDS, and XPS characterization of coatings obtained on titanium during AC plasma electrolytic process enriched in magnesium. *Advances in Materials Science* **18**, 68-78, (2018).
37. Wild, M. *et al.* Lithium sulfur batteries, a mechanistic review. *Energy Environ. Sci.* **8**, 3477-3494, (2015).
38. Clark, S. J. *et al.* First principles methods using CASTEP. *Z. Kristallogr.* **220**, 567-570, (2005).
39. Wang, C. *et al.* Unravel the Catalytic Effect of Two-Dimensional Metal Sulfides on Polysulfide Conversions for Lithium-Sulfur Batteries. *ACS Appl. Mater. Inter.* **12**, 43560-43567, (2020).
40. Perdew, J. P. *et al.* Atoms, molecules, solids, and surfaces: Applications of the generalized gradient approximation for exchange and correlation. *Phys. Rev. B* **46**, 6671-6687, (1992).
41. Rappe, A. M., Rabe, K. M., Kaxiras, E. & Joannopoulos, J. D. Optimized pseudopotentials. *Phys. Rev. B* **41**, 1227-1230, (1990).

Declarations

Acknowledgements

Z. M. and Y. L. gratefully acknowledge financial support from the Natural Sciences and Engineering Research Council (NSERC) of Canada through the Discovery Grants (RGPIN-2016-04366) and the Strategic Partnership Grants for Projects (STPGP 521458) programs. Z. Z. gratefully acknowledge financial support from the National Natural Science Foundation of China (No. 21776197 and 22078214).

Author contributions

Z. M. and Y. L. developed the concept. Z. M. conducted the experiments and analyzed the data. Z. Z. carried out the DFT calculations. Z. M. and Y. L. co-wrote the manuscript. All the authors discussed the results and commented on the manuscript.

Additional information

Supplementary information is available for this paper at

Competing financial interests

The authors declare no competing financial interests.

Figures

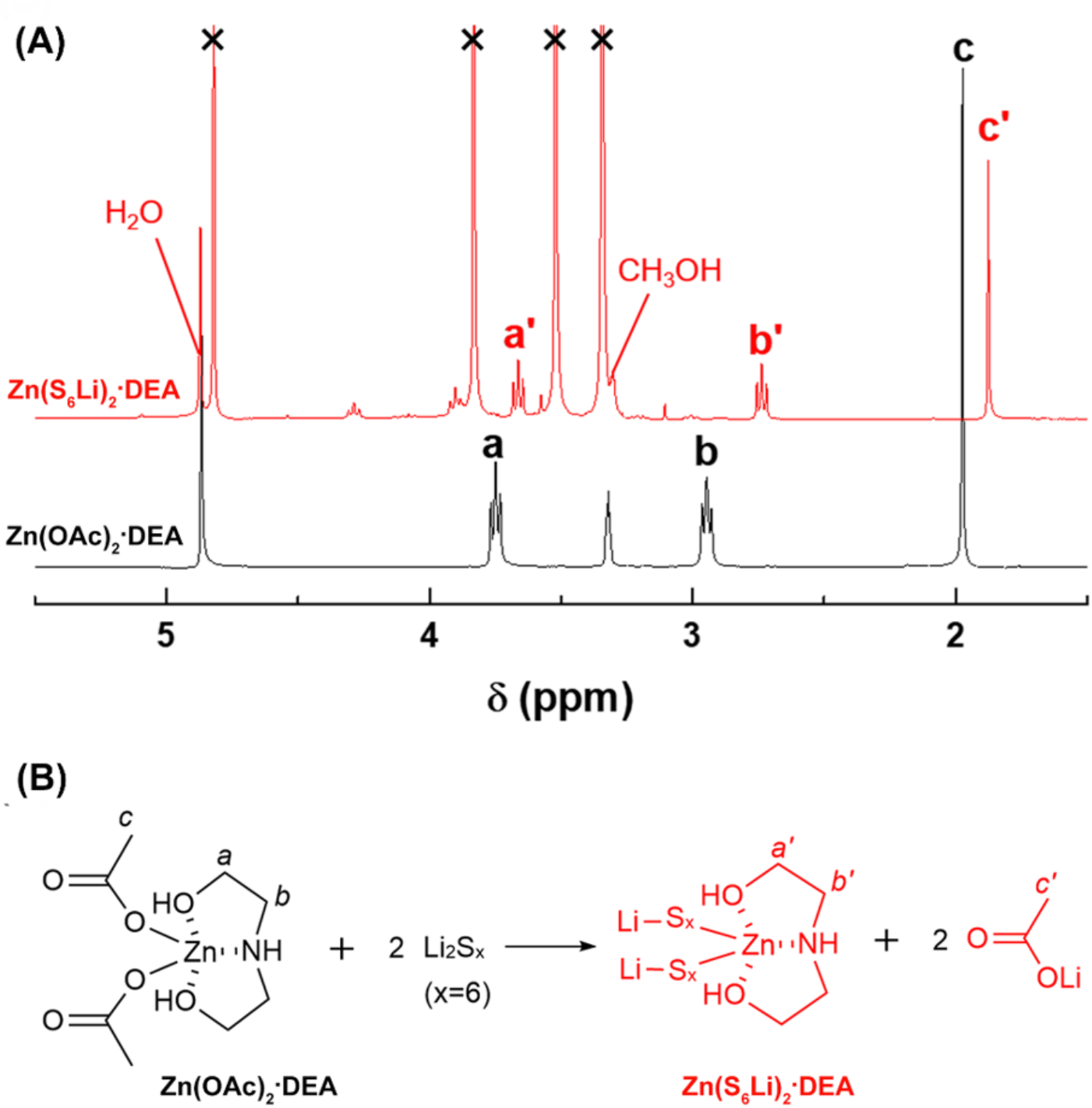

Figure 1

The interaction between Zn(OAc)2·DEA and Li2S6. (A) 1H NMR spectra of Zn(OAc)2·DEA in CD3OD (prepared in CD3OD) before and after addition of 2 eq. of Li2S6. Peaks with "□" are from solvents (DOL/DME) present in Li2S6 (Fig. S2D). (B) The proposed reaction between Zn(OAc)2·DEA and 2eq. of Li2S6.

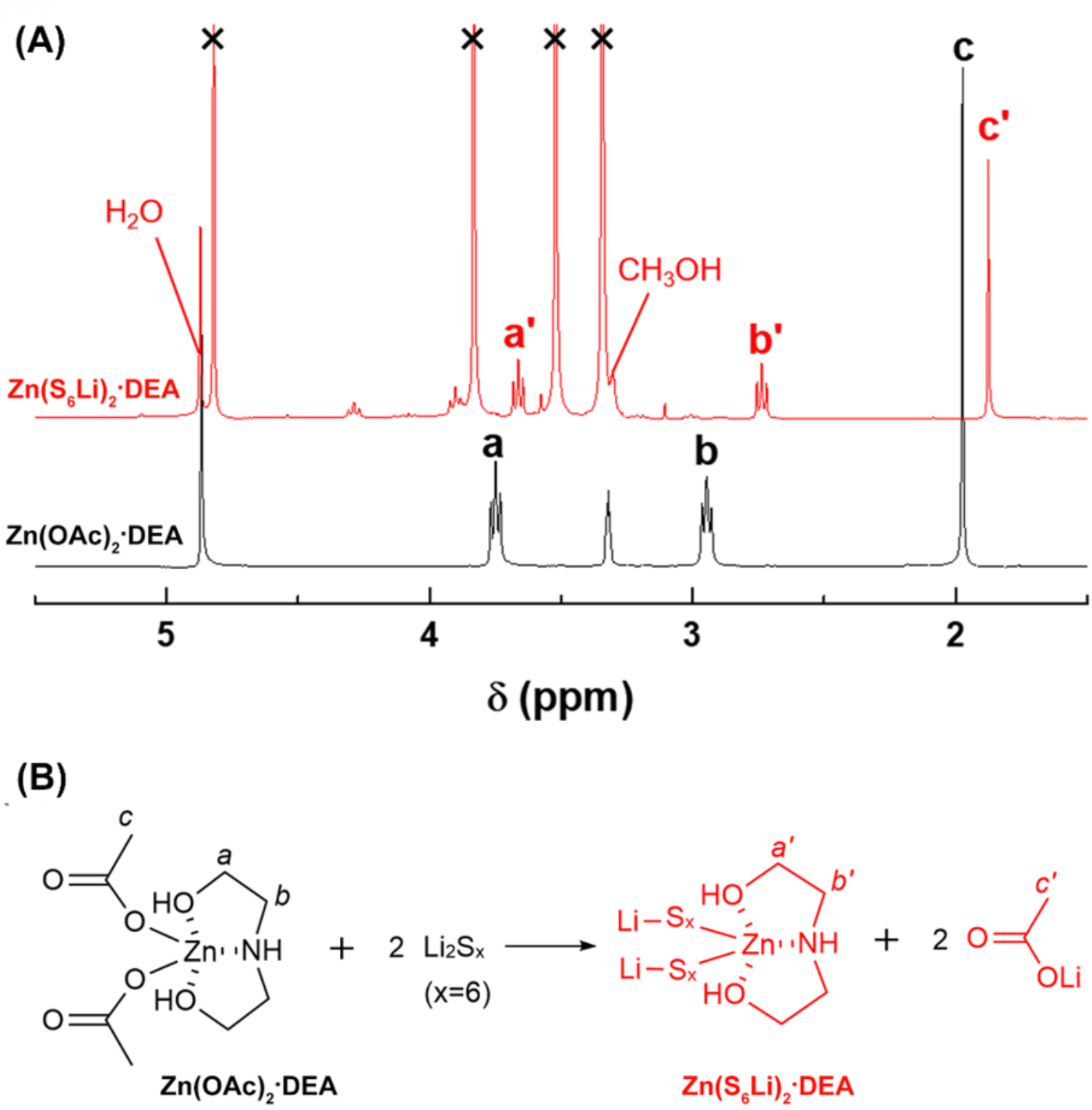

Figure 1

The interaction between Zn(OAc)2·DEA and Li2S6. (A) 1H NMR spectra of Zn(OAc)2·DEA in CD3OD (prepared in CD3OD) before and after addition of 2 eq. of Li2S6. Peaks with "□" are from solvents (DOL/DME) present in Li2S6 (Fig. S2D). (B) The proposed reaction between Zn(OAc)2·DEA and 2eq. of Li2S6.

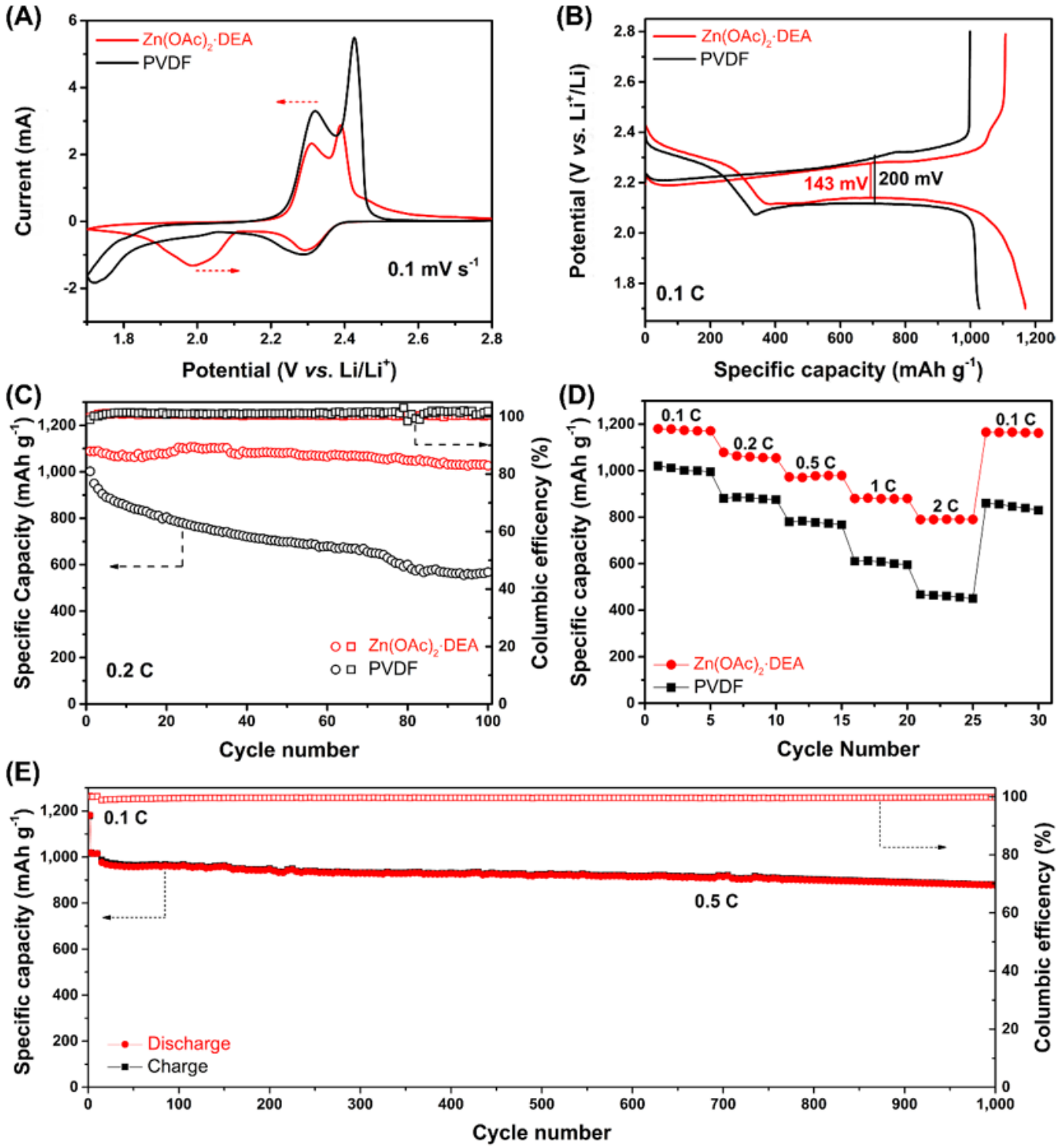

Figure 2

Electrochemical performance of sulfur electrodes using Zn(OAc)2·DEA as binder. (A) CV curves at a scan rate of 0.1 mV s-1. (B) Discharge-charge profiles at 0.1 C. (C) Cycling performance at 0.2 C. (D) Rate performance of Zn(OAc)2·DEA and PVDF based electrodes at different rates. (E) Long-term cycling performance of Zn(OAc)2·DEA based electrode at 0.5 C, where the first cycle was performed at 0.1 C for activation.

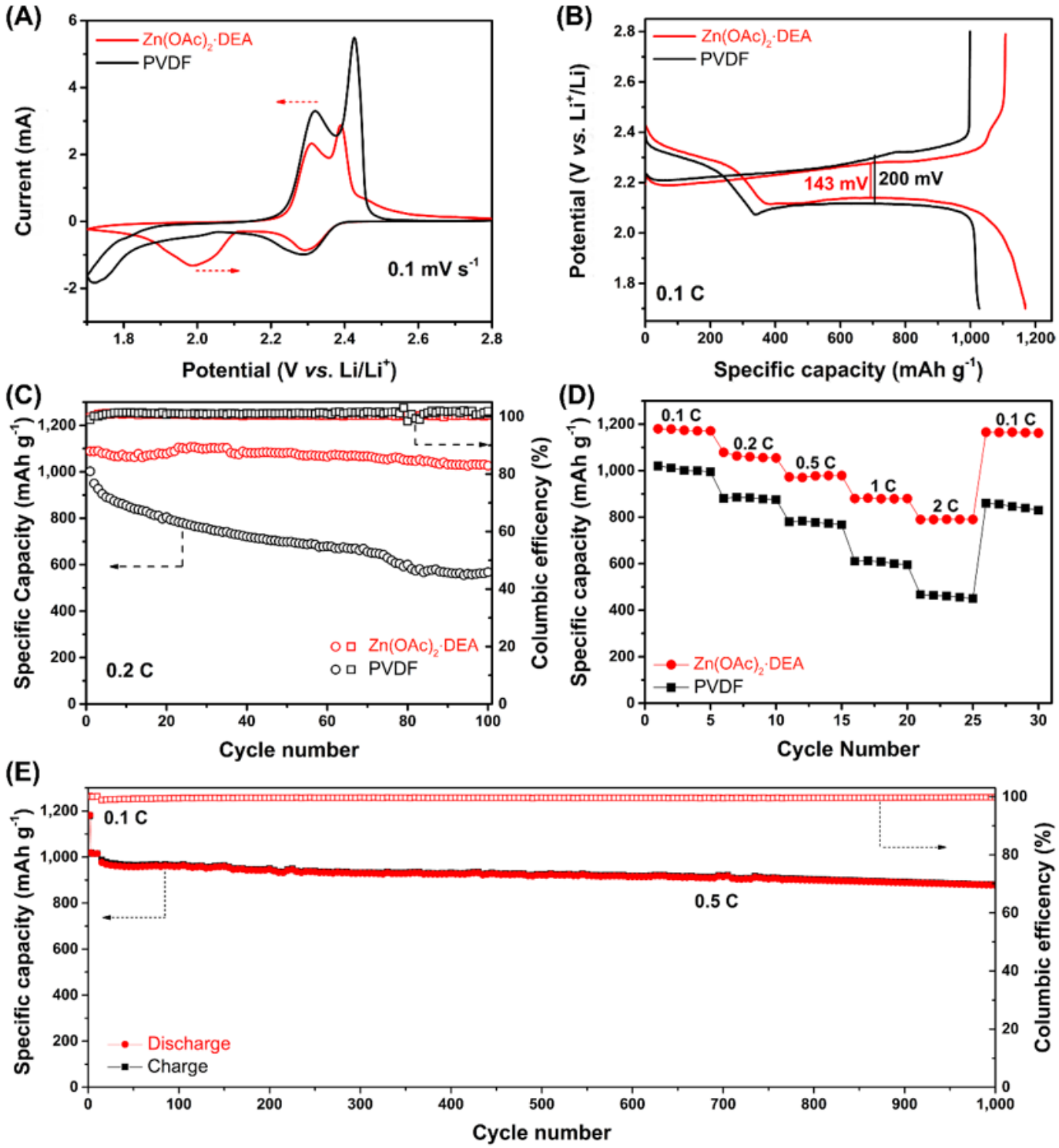

Figure 2

Electrochemical performance of sulfur electrodes using Zn(OAc)2·DEA as binder. (A) CV curves at a scan rate of 0.1 mV s-1. (B) Discharge-charge profiles at 0.1 C. (C) Cycling performance at 0.2 C. (D) Rate performance of Zn(OAc)2·DEA and PVDF based electrodes at different rates. (E) Long-term cycling performance of Zn(OAc)2·DEA based electrode at 0.5 C, where the first cycle was performed at 0.1 C for activation.

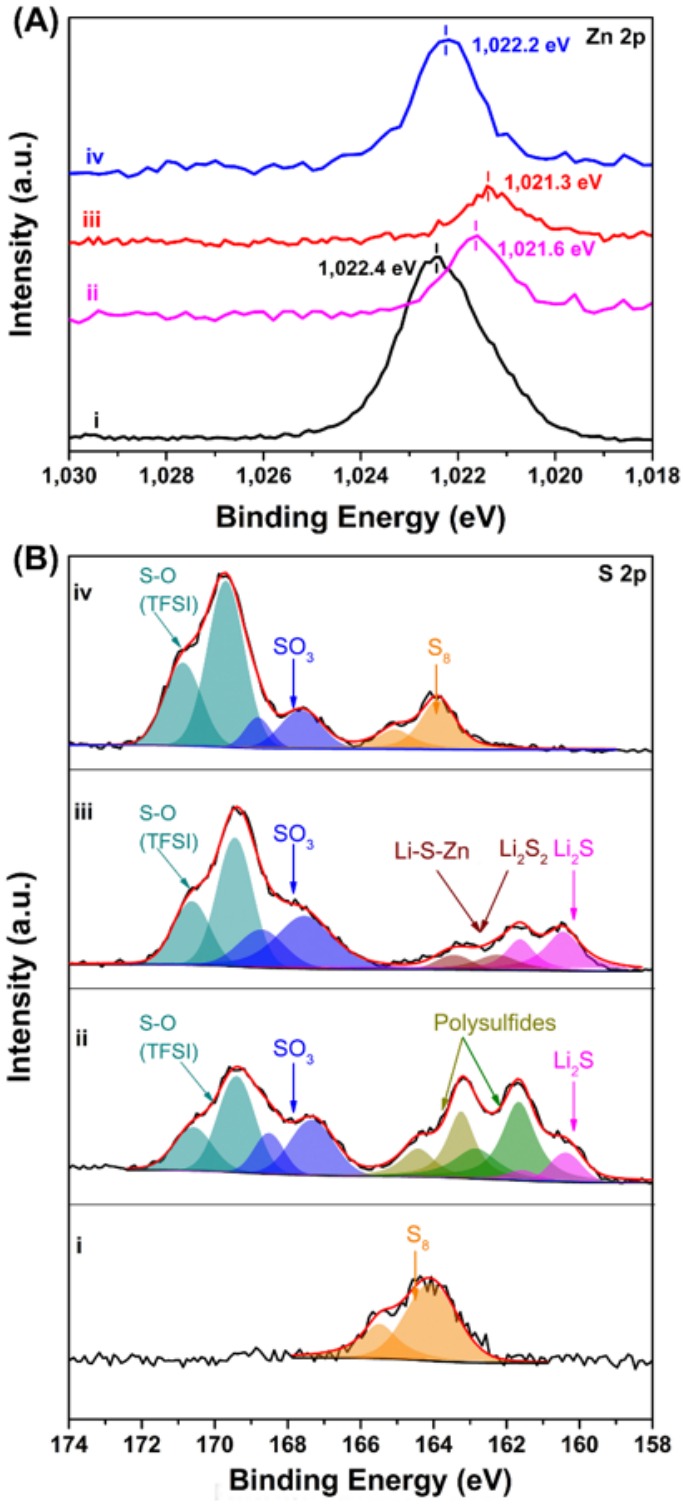

Figure 3

XPS spectra of Zn(OAc)2·DEA electrodes under different states. (A) Zn 2p and (B) S 2p (i: fresh electrode, ii: discharge to 2.2 V, iii: discharge to 1.7 V and iv: charge to 2.8 V).

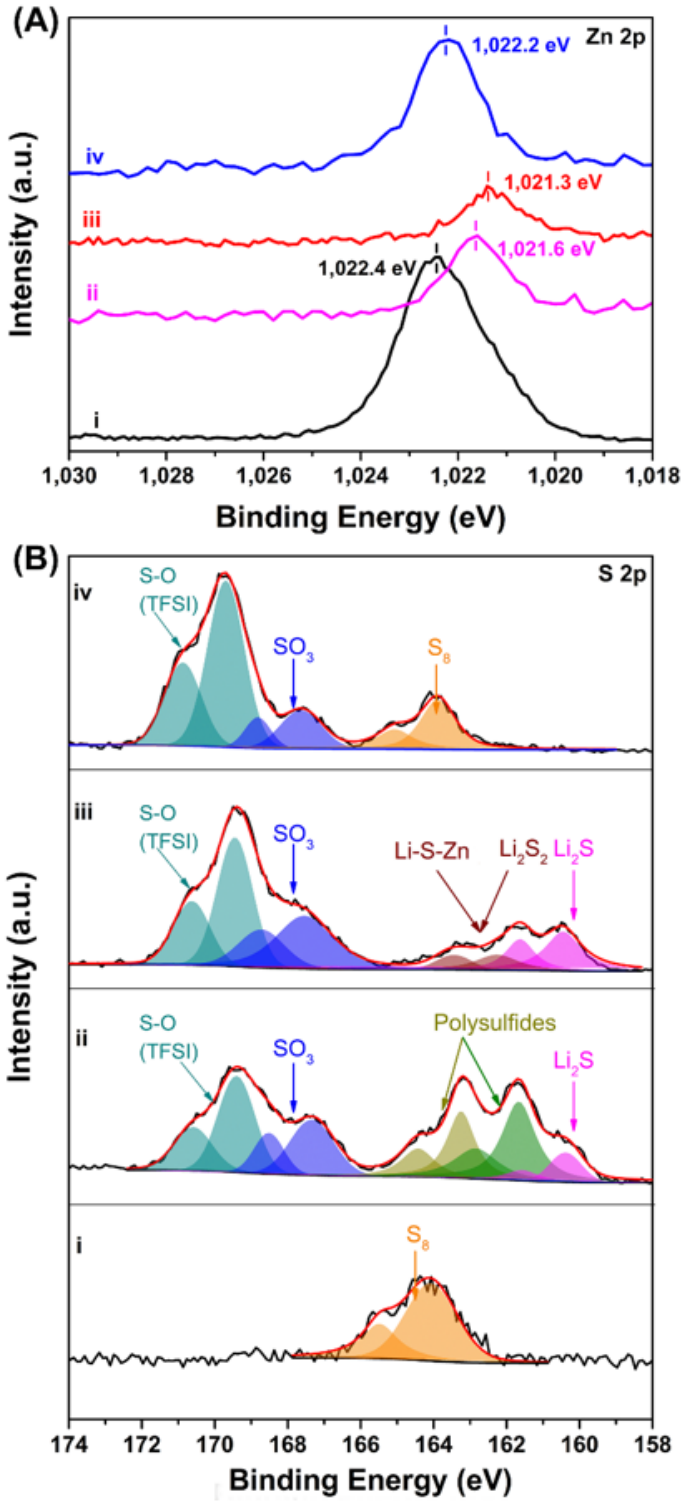

Figure 3

XPS spectra of Zn(OAc)2·DEA electrodes under different states. (A) Zn 2p and (B) S 2p (i: fresh electrode, ii: discharge to 2.2 V, iii: discharge to 1.7 V and iv: charge to 2.8 V).

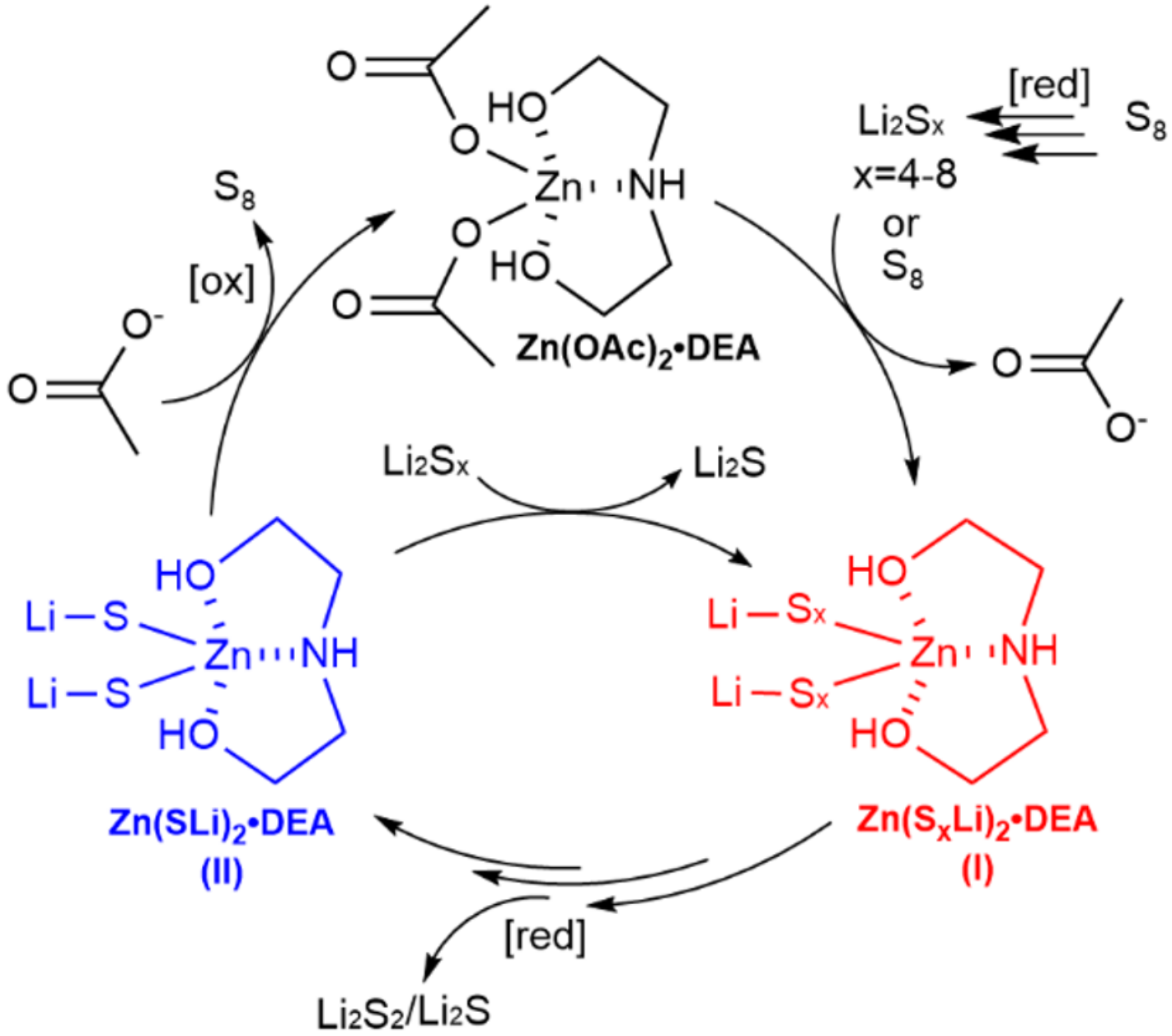

Figure 4

Proposed reaction cycle of Zn(OAc)2·DEA during discharge/charge processes of the Zn(OAc)2·DEA based sulfur electrode ([red]: reduction, [ox]: oxidation).

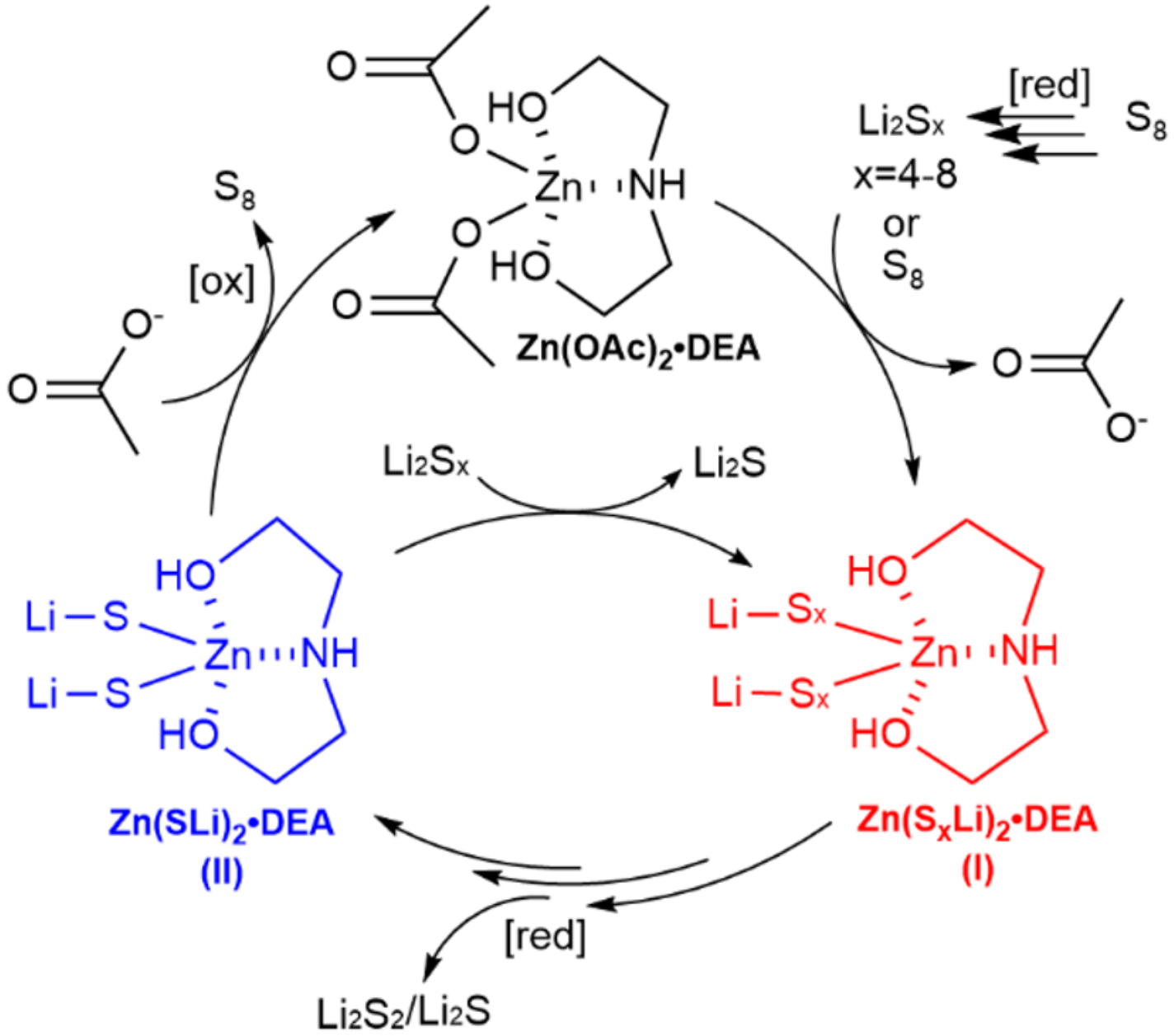

Figure 4

Proposed reaction cycle of Zn(OAc)2·DEA during discharge/charge processes of the Zn(OAc)2·DEA based sulfur electrode ([red]: reduction, [ox]: oxidation).

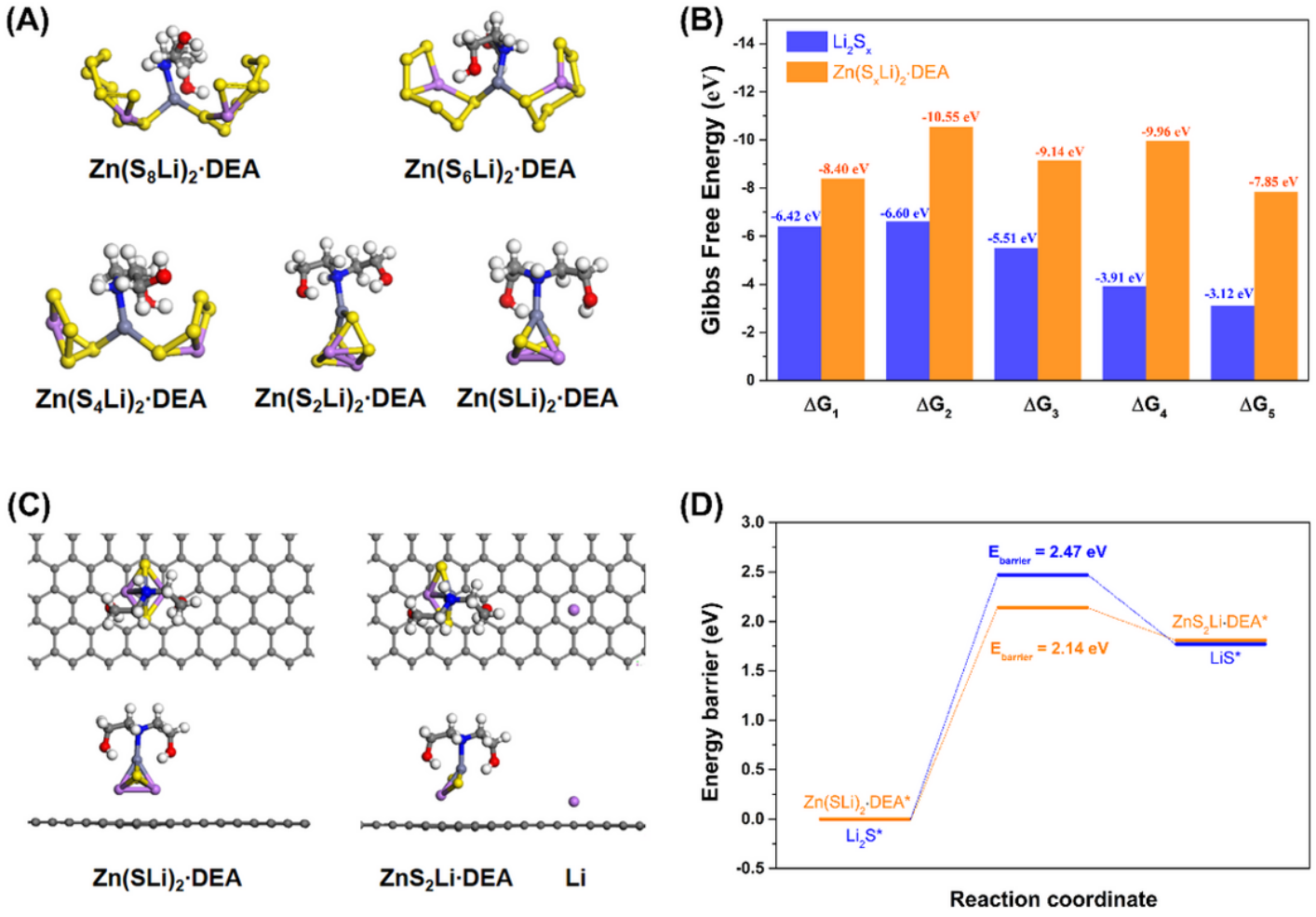

Figure 5

Improved kinetics of sulfur reactions with Zn(OAc)2·DEA. (A) The optimized geometries of complexes of Zn2+·DEA and different sulfides. (B) The Gibbs free energy of the reduction reductions (only products shown; see Supplementary Information for detailed reactions) of different sulfur species based on DFT calculations. (C) The initial (left) and final (right) structures in the dissociation of Zn(SLi)2·DEA on a graphene substrate. (D) Energy profiles of the dissociation of Li2S (blue) and Zn(SLi)2·DEA (II) (orange) on graphene, whereas the initial (left) and final (right) structures in the dissociation of Zn(SLi)2·DEA (II) are on graphene substrate. The grey, red, white, yellow, purple, dark blue, and grey blue balls represent C, O, H, S, Li, N, and Zn atoms, respectively, in A and C.

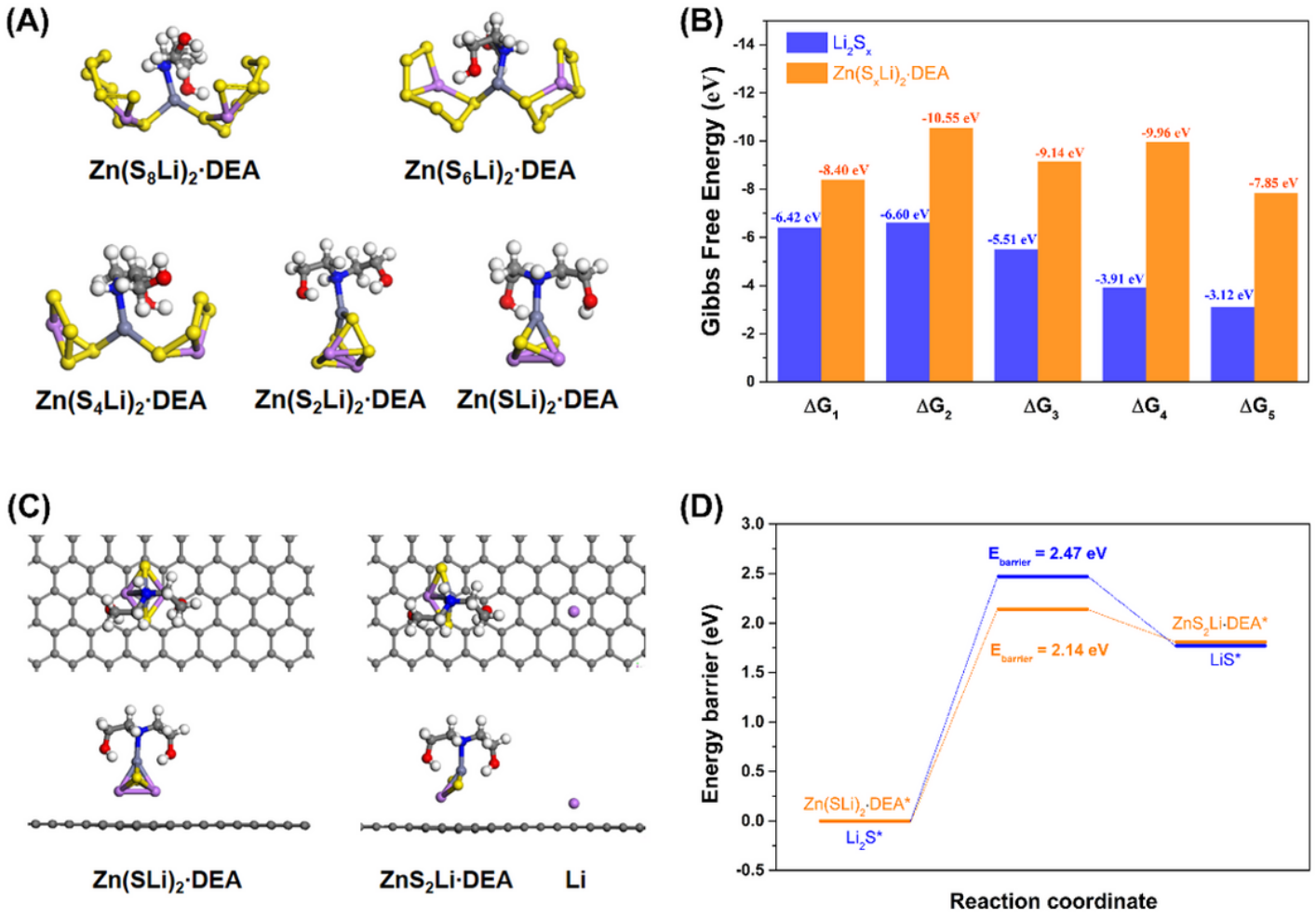

Figure 5

Improved kinetics of sulfur reactions with Zn(OAc)2·DEA. (A) The optimized geometries of complexes of Zn2+·DEA and different sulfides. (B) The Gibbs free energy of the reduction reductions (only products shown; see Supplementary Information for detailed reactions) of different sulfur species based on DFT calculations. (C) The initial (left) and final (right) structures in the dissociation of Zn(SLi)2·DEA on a graphene substrate. (D) Energy profiles of the dissociation of Li2S (blue) and Zn(SLi)2·DEA (II) (orange) on graphene, whereas the initial (left) and final (right) structures in the dissociation of Zn(SLi)2·DEA (II) are on graphene substrate. The grey, red, white, yellow, purple, dark blue, and grey blue balls represent C, O, H, S, Li, N, and Zn atoms, respectively, in A and C.

Supplementary Files

This is a list of supplementary files associated with this preprint. Click to download.

- ZnSupplementaryInformation.pdf
- ZnSupplementaryInformation.pdf

- MovieS1.mp4
- MovieS1.mp4
- MovieS2.mp4
- MovieS2.mp4
- MovieS3.MP4
- MovieS3.MP4
- MovieS4.mp4
- MovieS4.mp4